Exploring mesoscopic mass transport effects on electrocatalytic selectivity

Hendrik H. Heenen,* Hemanth S. Pillai, Karsten Reuter, and Vanessa J. Bukas*

Fritz-Haber-Institut der Max-Planck-Gesellschaft, Faradayweg 4-6, D-14195 Berlin, Germany

E-mail: heenen@fhi.mpg.de; bukas@fhi.mpg.de

Abstract

Electrocatalytic selectivity has shown a puzzling dependence on experimental parameters related to catalyst morphology or the reactor design. In this study, we explore the proposition that these effects are due to mesoscopic mass transport. Basis for the underlying mechanism is the kinetic competition that arises from exchanging surface-bound, yet volatile, reaction intermediates between the electrode and the bulk electrolyte. The electrocatalyst's morphology can be decisive in driving this competition since its surface area directly affects the probability that a diffusing species will return to the surface for continued reaction, rather than escape as an early partially-converted product. We argue that this competition is relevant for a number of technologically important reactions, including e.g. different products during the electrochemical CO_2 reduction on Cu-based catalysts. Combining microkinetic and transport modeling in a multi-scale approach, we specifically explore and quantify this effect for various showcase examples in the experimental literature. Despite its simplicity, our model correctly reproduces selectivity trends with respect to electrode potential and catalyst roughness. Comparing against experimental data further establishes catalyst roughness as a descriptor that unifies the effects of meso-, micro- and atomic-scale morphology on

selectivity through transport. The resulting insight provides an alternative or, at least, complementary explanation to changes in electrocatalytic selectivity that have otherwise been attributed to nano-structuring of active sites or electronic effects due to doping or alloying.

Main

Heterogeneous electrocatalysis is at the heart of developing sustainable energy technologies. The rational design of more efficient electrocatalysts, however, hinges upon improving our fundamental understanding of the underlying reaction mechanisms. At the microscopic level, these mechanisms are currently almost exclusively discussed through the lens of the catalytically active site.[1] The emerging mechanistic picture is one that is entirely focused on surface-bound reaction intermediates and the simple assumption that catalytic rates are directly controlled through the adsorption strength of these intermediates. Subsequent catalyst design strategies therefore revolve around tuning the nature of the active site, e.g. through doping or alloying. This approach has been met with tremendous success in predicting activity trends across different catalysts in computational screening studies for e.g. the electrochemical oxygen reduction reaction (eORR),[2–4] CO_2 reduction reaction (eCO_2RR),[5–7] and many others.[1] It has been known to fail, however, when it comes to more subtle aspects of the electrochemical kinetics. Such aspects can be decisive in determining the reaction path that is being followed and thus the final product that is being formed. Increasing experimental evidence, for example, shows electrocatalytic selectivity change with catalyst loading or reactor design in a non-obvious way that cannot be simply rationalized through considerations of the active site and its immediate chemical environment. Such puzzling effects bring the active site model into perspective and suggest a possibly important mechanistic role for mesoscopic mass transport phenomena.[8,9]

Mesoscopic mass transport can influence electrocatalytic processes in different ways. Diffusion limitations of reactants/products as well as so-called "local pH" effects are gaining

increasing attention,[8,10–14] especially in light of the urgent drive to upscale electrochemical process designs in recent years. We will focus here, however, on a considerably less studied effect of mass transport: the kinetic competition that arises from exchanging volatile reaction intermediates between the electrocatalyst surface and bulk electrolyte. This reaction model was first proposed by Behm *et al.* and coined the "desorption–re-adsorption–reaction" mechanism.[15–17] Basis for the underlying mechanism is the desorption of a specific surface-bound and usually closed-shell reaction intermediate, whose subsequent fate creates a bifurcation in the reaction pathway: either to re-adsorb onto the surface toward full conversion, or to entirely diffuse away and thus be detected as an early partially-converted product. Electrocatalytic selectivity is thus driven by the competition between surface kinetics and diffusion. Given this competition, descriptors of a catalyst's morphology such as the catalyst loading or inter-particle distance become critical as they directly affect the probability of re-adsorption, i.e. the probability that the diffusing species returns to the surface for continued reaction rather than escaping as an early intermediate product.

While largely overlooked, there have been some experimental reports recognizing the role of the "desorption–re-adsorption–reaction" mechanism in individual cases. In their original work, Behm *et al.* purposefully manipulated the catalyst loading to demonstrate how selectivity depends upon surface roughness during the eORR on Pt[17] as well as the electrochemical oxidations of methanol (eMeOHox)[15] and ethanol (eEtOHox).[16] More recently, similar mechanistic arguments were made to explain the varying selectivity towards CO during the eCO_2RR on Cu when changing the catalyst morphology (via e.g. nanoparticle coverage, distance, shape, and size)[18–20] or the reactant stream in reactor setups.[21–23] And yet, the impact of the "desorption–re-adsorption-reaction" mechanism as well as its generalization across different processes and systems remain unclear.

In this study, we demonstrate the role of mesoscopic mass transport in determining electrocatalytic selectivity for a number of technologically important processes, including the eORR and different products of eCO_2RR on Cu. Quantitative understanding of the under-

lying "desorption–re-adsorption–reaction" mechanism is established, for the first time to our knowledge, by developing a simple multi-scale model that couples diffusion to the electrochemical surface kinetics. Our model correctly reproduces a series of trends found in the experimental literature, while providing an alternative or, at least, complementary explanation to changes in electrocatalytic selectivity beyond the active site model. Within this picture, the electrode surface roughness emerges as a descriptor of selectivity that effectively captures the influence of catalyst morphology across multiple length-scales: the mesoscopic scale at the inter-particle level, microscopic scale at the intra-particle level, and nanoscopic scale at the atomic level. Our analysis finally highlights the relevance of the "desorption–re-adsorption–reaction" mechanism in catalyst degradation as morphological changes over time (e.g. due to nanoparticle agglomeration) induce corresponding changes in electrocatalytic selectivity.

"Desorption–re-adsorption–reaction" mechanism: A simple kinetic model

The "desorption–re-adsorption–reaction" mechanism describes the fate of a specific surface-bound, yet volatile, intermediate along the reaction path. The mechanism is schematically illustrated in Fig. 1 where this key intermediate X* (superscript * denotes an adsorbed configuration) faces a branching in the reaction path to either (i) continue along the potential-dependent surface route towards full catalytic conversion, or (ii) desorb above the surface where it starts to build up a local concentration gradient. In the second case, if diffusion is fast enough, the near-surface species $X^{(*)}$ will leave the surface entirely and be detected as an early partially-converted product X(aq) in the bulk (aqueous) solvent. If diffusion is relatively slow, however, $X^{(*)}$ faces the prospect of re-adsorbing onto the surface where it will once again be subjected to the (i) *vs* (ii) competition described above. The mechanism thus essentially boils down to a competition between surface kinetics and diffusion. To describe

this competition, we couple these two key components within a simple kinetic model of the selectivity-determining step.

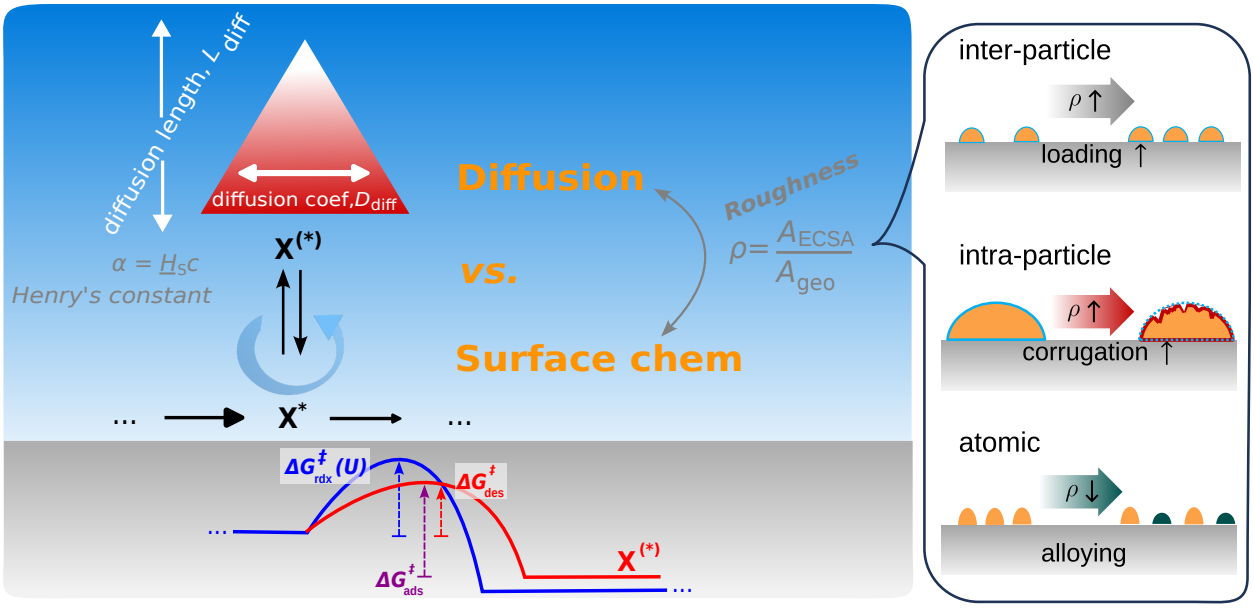

Figure 1: Schematic representation of the "desorption–re-adsorption–reaction" mechanism. A surface-bound, closed shell intermediate X* faces the kinetic competition between a forward surface redox step *vs.* desorption. Following desorption, if diffusion is fast enough, near-surface $X^{(*)}$ species will escape into the bulk electrolyte and be detected as an early, partially-converted product. Our model couples diffusion with the surface kinetics via the surface roughness ρ which effectively captures the influence of catalyst morphology across multiple length-scales: at the inter-particle (via e.g. catalyst loading), intra-particle (via e.g. microscopic surface roughening), and atomic (via alloying) levels. Additionally shown are the other six parameters entering our model: free-energy barriers ($\Delta G^{\ddagger}_{\mathrm{rdx}}(U)$, $\Delta G^{\ddagger}_{\mathrm{des}}$, $\Delta G^{\ddagger}_{\mathrm{ads}}$), as well as diffusion-related properties (D_{diff}, L_{diff}, H_{s}) as described in the text.

We describe the surface reaction steps through a mean-field microkinetic model, while mass transport is simply included as one-dimensional Fickian diffusion (in the direction perpendicular to the surface). The two model components are then coupled via the flux of species $X^{(*)}$ and we solve the problem iteratively for steady-state solutions. In practice, the steady-state assumption reduces the transport modeling to a simple analytical expression of Fick's first law.[24] A converged solution is one where the diffusion flux J_{diff} of species $X^{(*)}$ equals the corresponding flux output from the microkinetic model J_{mkm} (=turnover frequency $\times$ active site density) after normalizing the rate to account for the density of catalytically

active sites:

$$\frac{J_{\mathrm{mkm}}}{J_{\mathrm{diff}}} = \rho := \frac{A_{\mathrm{ECSA}}}{A_{\mathrm{geo}}} \tag{1}$$

Here the normalizing factor ρ represents the catalyst roughness, defined as the ratio of the electrochemically active surface area (ECSA) to the geometric surface area of the electrode. Roughness thus enters the model as a central key parameter, designed to effectively capture the influence of catalyst morphology on the resulting product selectivity. Importantly, as a commonly measurable quantity (e.g. through capacitive charging, or measured current densities), this parameter ρ also allows us to draw a direct relation to experimental trends in the following.

Apart from the electrocatalyst roughness, we include six additional parameters in our model. Three of these parameters enter the microkinetic model as the activation free energies for each of the competing surface reaction steps: the redox barrier $\Delta G^{\ddagger}_{\mathrm{rdx}}(U)$ for further electrocatalytic conversion of X* at the surface, the barrier $\Delta G^{\ddagger}_{\mathrm{des}}$ for X* desorption, and the reverse barrier $\Delta G^{\ddagger}_{\mathrm{ads}}$ for $\mathrm{X}^{(*)}$ adsorption. Among these barriers, we assume that only $\Delta G^{\ddagger}_{\mathrm{rdx}}$ depends on the applied electrode potential U, while desorption/adsorption are treated as purely 'chemical' steps and thus entirely independent of potential. This is an important distinction to make as it suggests that U can change selectivity by shifting the competition toward or against the surface redox reaction.[9,25] Again, this is a dependence that we will rely upon in the following when comparing against experimental selectivity data. Finally, the remaining three model parameters are part of the transport modeling: the diffusion coefficient D_{diff} and diffusion length L_{diff} of species $\mathrm{X}^{(*)}$ (which simplify the otherwise complex hydrodynamic dimensionless constants), as well as Henry's solubility constant H_{s} which is used to convert between activity and concentration. Further details on our kinetic model can be found in the SI, Sec. S1.

Screening the above model parameters allows to explore their effect on selectivity within the "desorption–re-adsorption–reaction" mechanism. Our sensitivity analysis (SI, Sec. S1.3)

shows the most dramatic, exponential dependence coming from the competing reaction barriers $\Delta G^{\ddagger}_{\mathrm{rdx}}(U)$, $\Delta G^{\ddagger}_{\mathrm{des}}$, and $\Delta G^{\ddagger}_{\mathrm{ads}}$, as well as from the electrode potential U (indirectly through $\Delta G^{\ddagger}_{\mathrm{rdx}}$). This exponential dependence follows that of the resulting reaction rates and can change the selectivity towards X(aq) from 100% to 0% within only few hundred millivolts of increasing overpotential (SI, Fig. S2). In comparison, the effect from varying catalyst morphology is weaker and emerges as an asymptotic $\propto 1/\rho$ dependence in selectivity. This relation is founded in the competition between diffusion and re-adsorption: the probability of $\mathrm{X}^{(*)}$ re-adsorption increases linearly with ρ, thus leading to more of the final product and less of the volatile intermediate product. Albeit weaker than the dramatic response to U, the role of ρ can still be crucial to catalytic performance as will be demonstrated in the following. Finally, when chosen within physically reasonable ranges (SI, Fig. S2), the remaining transport-related parameters (D_{diff}, L_{diff}, and H_{s}) generally influence selectivity to a much lesser extent. For example, exchanging the D_{diff} value of acetaldehyde (13.75 x $10^{-10}\,\mathrm{m}^2\cdot\,\mathrm{s}^{-1}$) to that of CO (20.3 x $10^{-10}\,\mathrm{m}^2\cdot\,\mathrm{s}^{-1}$) will typically only increase selectivity towards the diffusing intermediate product by <10%.

In the following, we focus on ρ and (to a second extent) U as variables against which to predict selectivity for several showcase catalytic reactions. As already indicated, the reasons for this choice include (i) the strong influence of these two parameters on selectivity with asymptotic and exponential behaviors, respectively, according to $\propto \frac{\exp(-U)}{\rho}$, as well as (ii) the ability to draw a direct connection to measurable experimental variables. The remaining model parameters are then either taken from the literature or approximated to fit experiment (SI, Sec. S1.4). Values for the activation free energies in particular, as well the potential-dependent $\Delta G^{\ddagger}_{\mathrm{rdx}}(U)$ functional form, are unfortunately mostly unavailable and are thus fitted to reproduce measured selectivity curves. It is important to stress, however, that the effect of ρ in these situations is always simulated by consistently re-using the same set of parameters within each reaction model studied. This allows for an unbiased comparison of the results when specifically focusing on the response to varying catalyst morphology.

We explore this effect in the next sections as it arises from surface roughening on different catalyst length-scales: the inter-particle, intra-particle, and atomic levels.

Selectivity changes with electrocatalyst morphology

The effect of catalyst loading

We first consider selectivity as a function of catalyst coverage or loading on the electrode support. This effect corresponds to catalyst roughening at the particle level and has been systematically investigated by the group of Behm for different electrocatalytic reactions on Pt electrodes. Figure 2 shows digitized data from two such experimental studies for the (a) eORR on polycrystalline Pt disks[17] (top), and (b) eMeOHox on Pt nanoparticles[15] (bottom). Both of these reactions involve volatile intermediates that may give rise to early, partially-converted products following the "desorption–re-adsorption–reaction" mechanism. We therefore want to examine the yield towards these early products *vs.* all later products that can appear further down the reaction path: hydrogen peroxide (H_2O_2) *vs.* water in the case of eORR, and formaldehyde (CH_2O) *vs.* formic acid (HCOOH) plus CO_2 in the case of eMeOHox (SI, Sec. S2.1). It is exactly this selectivity that is plotted in Figs. 2(a) and 2(b), respectively, as a function of the electrocatalyst roughness ρ. The roughness parameter was purposefully manipulated during these experiments by carefully controlling the Pt catalyst loading and is measured here either against a planar electrode surface (for which ρ=1 is assumed) in Fig. 2(a) or normalized by mass (such that ρ=1 corresponds to the lowest mass loading experiment of 7 μg/cm^2 Pt) in Fig. 2(b). Either way, the resulting data clearly show that catalyst roughening decreases the selectivity towards the early, partially-converted (H_2O_2 or CH_2O) product.

The mechanistic picture emerging from the two case studies presented in Fig. 2 is perfectly consistent with the "desorption–re-adsorption–reaction" mechanism. Following the rationale provided by Behm *et al.*, higher catalyst loading means smaller distance between

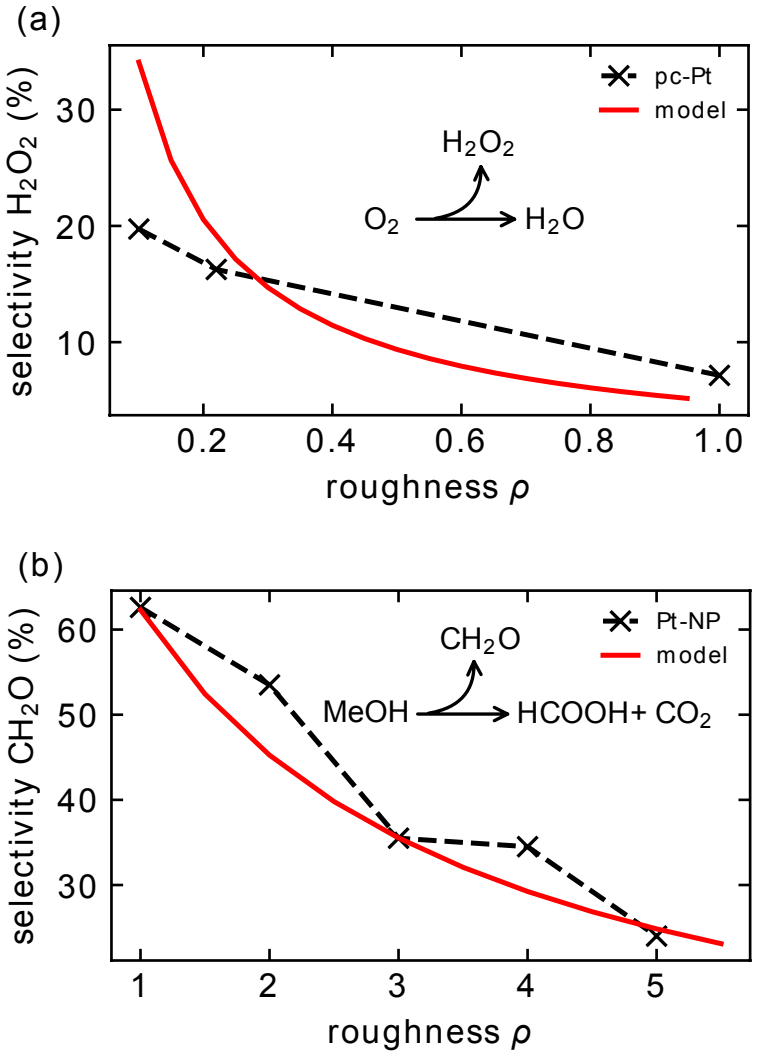

Figure 2: Selectivity towards the early, partially-converted products (a) H_2O_2 during the eORR and (b) CH_2O during eMOHox, as a function of catalyst roughness ρ. Solid red lines show predictions from our kinetic model, while black 'x' markers represent experimental data adapted from Refs. 17 and 15, respectively. The dashed lines are meant to guide the eye. Experimental catalyst morphologies are (a) polycrystalline (pc) Pt disks for which we reference ρ against a planar (ρ=1) electrode surface, and (b) Pt nanoparticles (NP) where we normalize ρ by measured catalyst mass. For further details, cf. SI, Sec. S3.1.

neighboring particles and thus a higher probability for diffusing intermediates to re-adsorb. More re-adsorption favors continued surface reaction and lowers the selectivity towards the partially-converted product. Considering its simplicity, our kinetic model captures this effect with almost remarkable agreement to experiment. The theoretical predictions (using model parameters listed in SI, Table S2) are represented by the solid red lines in Fig. 2 and show the anticipated $\propto 1/\rho$ dependence discussed in the previous section. These curves largely reproduce the experimental trends. Deviation is most noticeable only under conditions of ultra-low catalyst loading ($\rho < 0.2$) in Fig. 2(a). The model's over-estimation of the experimental H_2O_2 selectivity may be attributed to an inhomogeneous distribution of catalyst particles that cannot be described by our effective, one-dimensional ρ descriptor. The experiment-theory comparison is likely further skewed here by a more complex dependence on the applied electrode potential than that predicted by the "desorption–re-adsorption–reaction" mechanism (SI, Sec. S3.1). This potential dependence has been previously discussed for the Pt-based eORR as the result of multiple competing reaction paths (that do not go through the volatile H_2O_2 intermediate),[17] but such mechanistic intricacies go well beyond the scope of our simple model and are not further discussed.

The effect of catalyst particle shape and surface corrugation

We next explore selectivity with varying catalyst particle shape and surface corrugation, i.e. the influence of morphological features on the mesoscopic/microscopic range. These effects are demonstrated here for the eCO_2RR on Cu electrodes; a model system of immense technological importance due to its unique ability to synthesize both a variety of one-carbon (C_1), but also high-value multicarbon (C_{2+}) products. A study by the group of Jaramillo *et al.* identified and enumerated a total of 16 different possible products,[26] of which we classify about half as the closed-shell intermediates that may be relevant to the "desorption–re-adsorption–reaction" mechanism. It is this intricate reaction network, along with the plethora of available experimental data, that make Cu-based eCO_2RR an ideal playground

to explore the effects of mass transport on electrocatalytic selectivity. In this section, we specifically focus on two such intermediates in the reaction mechanism: CO as the prominent first product following CO_2 electroreduction,[27] and acetaldehyde (MeCHO) which appears further down the reaction path and competes with various other C_{2+} products.[28–31]

Figure 3 compiles selectivity data from different experimental studies, with very different catalyst morphologies. A Cu(111) single crystal,[32] polycrystalline Cu foil (pc-Cu),[26] as well as two sets of data for oxygen-derived Cu (OD-Cu)[32,33] are all included in Fig. 3(a). This figure panel plots the selectivity towards CO (*vs.* all later C_1 plus C_{2+} products) as a function of the applied electrode potential U_{SHE} (referenced against the standard hydrogen electrode, SHE). All datasets for the different Cu catalysts are found to show a very similar exponential drop ($\propto \exp\left(-U_{\mathrm{SHE}}\right)$) in CO selectivity with increasingly reducing potentials. This effect can be simply explained on the basis of the "desorption–re-adsorption–reaction" mechanism: more reducing U_{SHE} drives forward the surface redox reaction, thus lowering the fraction of CO that desorbs and diffuses away. Using measured (total) current densities, we assign roughness values to the various Cu catalyst morphologies (SI, Secs. S2.2 & S3.2) and thus reveal a second very important trend. Based on their corresponding roughness, we find that the presented CO selectivity curves are sorted into two distinct groups: Cu(111) and pc-Cu datasets with $\rho \approx 1$ fall pretty much on top of one another, implying essentially the same electrocatalytic behavior due to surface restructuring under reaction conditions. With a higher ρ of about 30, however, the two curves representing the OD-Cu samples are clearly offset towards higher (less reducing) potentials. Again, in context of the "desorption–re-adsorption–reaction" mechanism, higher roughness means more re-adsorption and continued electrocatalytic conversion. As a result, at the same U_{SHE} value, OD-Cu has a lower affinity towards CO and higher affinity towards high-value C_{2+} products. Our kinetic model (solid lines in Fig. 3(a)) establishes this mechanistic picture. Using the exact same set of model parameters for all Cu catalysts (SI, Table S2) and varying only the ρ value between 1 and 30, reproduces the experimental offset between the two groups within semi-quantitative

agreement.

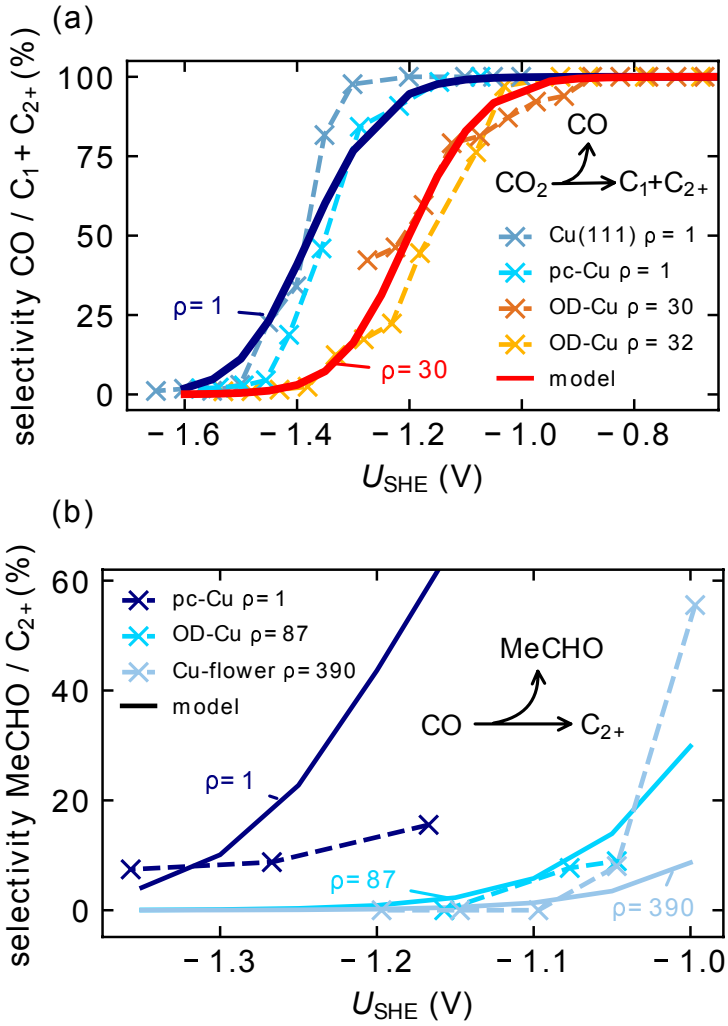

Figure 3: Selectivity towards (a) CO *vs.* later C_1/C_2+ products and (b) MeCHO *vs.* later C_2+ products, as a function of applied U_{SHE} potential during the eCO_2RR on different Cu catalysts. Solid lines show theoretical predictions when varying only the roughness parameter ρ within each of the (CO and MeCHO) kinetic models. All 'x' markers represent experimental data adapted from (a) Refs. 26, 32, 33 and (b) Refs. 28, 34, 35. The dashed lines are meant to guide the eye. Experimental ρ values are assigned based on measured (total) current densities, as marked in the figure's legend, with ρ=1 for polycrystalline (pc) Cu as reference. For further details, cf. SI, Sec. S3.2.

The generality of the "desorption–re-adsorption–reaction" mechanism is further strengthened by our second case study in Fig. 3(b). This figure panel plots the selectivity towards MeCHO (*vs.* later C_{2+} products) as a function of U_{SHE}, while similarly compiling experimental data on different Cu morphologies: a pc-Cu sample of ρ=1,[34] an OD-Cu sample of

ρ=87,[28] and a highly porous Cu nanoflower (Cu-flower) of ρ=390.[35] The exponential drop of MeCHO selectivity with reducing potentials is not as clear here as in the previous example due to the limited U_{SHE} range of the available experimental data. This relation is nevertheless predicted by our kinetic model (solid lines in Fig. 3(b)), along with the inverse relation with respect to catalyst roughness. While quantitative experiment-theory agreement is certainly far from perfect, the underlying trends are clearly compatible. Taken together, Fig. 3 confirms the prevalent notion that copper's meso- or microscopic morphology is critical to the resulting eCO_2RR selectivity. These effects have so far mostly been associated, however, with changes in the nature or population of active sites, such as e.g. undercoordinated steps and kinks, due to roughening.[36–39]

The effect of alloying

Our next and final case study addresses the effect of alloying. Alloying is often exploited in catalyst design as a tool that allows to manipulate the electronic properties, and hence reactivity, of the active site. This concept was recently invoked to rationalize the increased selectivity towards acetate (Ac) that was measured during CO electroreduction (eCORR) on two different Cu-based alloys, namely Cu-Pd[40] and Cu-Ag.[41] The authors of both these studies in fact found that there exists an optimal alloying ratio for which maximal selectivity towards this C_2 product is reached (SI, Sec. S3.3). They explained this on the basis of active site binding strengths. We argue here that modifying the density of active sites within the "desorption–re-adsorption–reaction" mechanism provides again an alternative, or at least complementary, reasoning to explain the reported selectivity changes.

In a combined experiment-theory study, some of us recently proposed that the mechanism for forming Ac on Cu is very much in line with the "desorption–re-adsorption–reaction" mechanism.[25] The case of Ac is just slightly more complicated by the fact that it is not directly acetate, but ketene, that desorbs from the surface. This earlier intermediate is then attacked by OH^- ions in the electrolyte to finally form Ac via a solution reaction step.

While this last step introduces an additional pH dependence (through the involvement of OH^-), the selectivity towards Ac is still driven by the competition between surface kinetics and diffusion. The resulting $\propto 1/\rho$ dependence on catalyst morphology thus provides a reasonable explanation for lower Ac yields measured on more roughened Cu electrodes.[25,42,43] Our present model thus suggests the inverse effect from Pd- or Ag-based alloying.

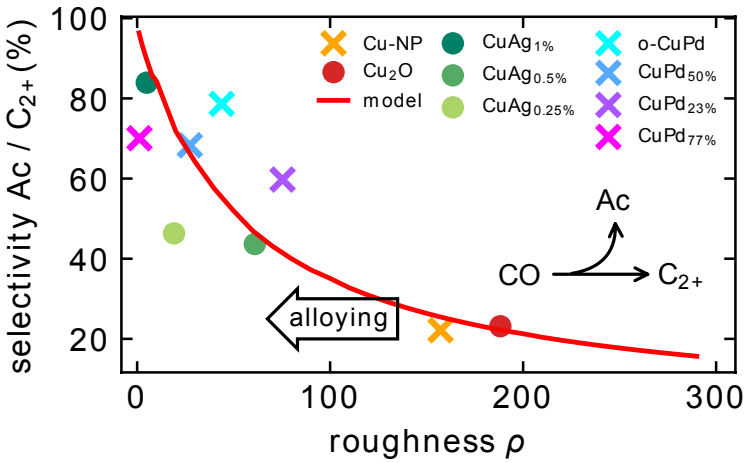

Figure 4: Selectivity towards acetate (Ac) *vs.* later C_2+ products during the eCORR on different Cu-based catalysts, as a function of catalyst roughness ρ. Data are shown for a constant (U_{SHE}=-1.7V) electrode potential. The solid red line shows the prediction of the kinetic model[25] when varying only the ρ parameter and keeping all other parameters fixed. The markers represent experimental data for Pd-based (crosses) and Ag-based (circles) Cu alloys with varying alloy ratios adapted from Refs 40 and 41, respectively. Additionally shown are data for an atomically ordered Cu-Pd intermetallic ('o-CuPd') as well as pure Cu nanoparticles (NP)[40] and Cu_2O[41] reference samples. All experimental ρ values are assigned based on measured (total) current densities. For further details, cf. SI, Sec. S3.3.

Alloying a Cu catalyst with Pd or Ag effectively lowers ρ (according to the definition in Eq. 1) due to the lower density of catalytically active sites, at least of those sites that are selective towards forming the late C_{2+} products against which we measure here. This relation is best illustrated in Fig. 4 which compares different Cu-based catalysts in terms of Ac selectivity (*vs.* later C_{2+} products) and "catalytically relevant" surface roughness at a fixed (U_{SHE}=-1.7V) potential. The markers represent the data from the two experimental studies with corresponding ρ values estimated from measured current densities (SI, Secs. S2.2 & S3.3): Cu-Pd catalyst samples (including both atomically ordered intermetallic 'o-

CuPd' and disordered 'CuPd$_{x\%}$' alloyed structures),[40] as well as Cu-Ag samples ('CuAg$_{x\%}$' alloys)[41] are included with different alloying ratios. These data are characterized by a much lower ρ as compared to their corresponding (non-alloy) Cu_2O[40] and (pure) Cu[41] reference samples. The higher ρ generally comes with lower Ac selectivity and we specifically outline a $\propto 1/\rho$ behavior, characteristic for the "desorption–re-adsorption–reaction" mechanism. This trend is well reproduced by the kinetic model[25] when only varying the ρ parameter and keeping all other parameters fixed (solid red line in Fig. 4). The emerging mechanistic picture is thus very simple as it reduces the effect of alloying to merely lowering ρ within the "desorption–re-adsorption–reaction" model. One may therefore even think of alloying as changing the atomic-scale roughness. Lower ρ ultimately means that more Ac will escape as an intermediate species when measured against later, further-reduced C_{2+} products. We therefore suggest that high Ac selectivity is not necessarily unique to Cu-based alloys, but may be expected also on pure Cu electrodes if the surface morphology remains smooth enough under reaction conditions. There exists some experimental evidence to support this hypothesis.[43,44] Finally, generalizing this alloying effect, we note that similar observations have been made by the group of Koper for the volatile CO product during the eCO_2RR on Cu-Zn alloys.[45]

Conclusions

This work calls attention to mesoscopic mass transport as a decisive factor in determining electrocatalytic selectivity. Through multi-scale modeling and a detailed inspection of the experimental literature, we quantify the effect of the so-called "desorption–re-adsorption–reaction" mechanism and show its generality over different redox reactions, different catalysts, and different electrode setups. Importantly, our analysis highlights surface roughness as a key descriptor that can capture the effect of catalyst morphology on selectivity across all relevant length scales. This simple picture thus reduces to (one-dimensional) roughness

any influence from morphology, regardless of its origin: catalyst loading, particle shape/size, surface corrugation due to e.g. oxidative pretreatment or electro-polishing, and even alloying.

We believe the present mechanistic insight holds value for electrocatalyst design, not only towards optimizing steady-state operation, but also in the context of catalyst aging and degradation. Roughness is, after all, most often a dynamic property under reaction conditions.[46–49] According to the "desorption–re-adsorption–reaction" mechanism, a dynamically evolving catalyst morphology (e.g. due to reconstruction, particle agglomeration, or dissolution) will change the resulting product selectivity and thus the targeted catalytic performance. We demonstrate this relation via e.g. time-dependent measurements during the eCO_2RR on differently sized Cu nanoparticles.[50] Following the same procedure as above to extract roughness estimates from experimental current densities, we find the expected trend for measured selectivity towards the intermediate CO product (SI, Sec. S4.1). Surface roughness decreases over time as Cu particles coalesce and this leads to a simultaneous ca. 10-20% increase in CO selectivity already within the first twelve hours of operation. A similar mechanistic picture emerges for the time-dependent selectivity towards H_2O_2 during the eORR on Pd[46] (SI, Sec. S4.2).

With the "desorption–re-adsorption–reaction" mechanism in mind, our final remark concerns system design strategies. In this study we purposefully put focus on catalyst morphology and, to a second extent, the electrode potential as tunable parameters that can control product selectivity. Correspondingly, we also limited our literature search to lab-scale studies that usually rely on conventional H-cell or flow cell setups. While such setups leave little room for manipulating the electrolytes' macroscopic hydrodynamics, this situation changes when up-scaling towards the practical device level.[21–23] Here, careful reactor design to control the diffusion properties of volatile intermediates may prove particularly important to the resulting selectivity. In this context, unexplored effects due to special pore catalyst geometries[10,12] or particle arrangements[20] that go beyond our simplified one-dimensional transport model open up exciting, new research avenues.

Methods

Our kinetic model was developed as an in-house implementation. The surface kinetics are simulated via a mean-field model and solved for steady-state using an ODE solver available in the SciPy distribution.[51] Mass transport is included as one-dimensional diffusion and described analytically via Fick's first law.[24] A boundary condition is set by assigning the bulk concentration of desorbing species to zero. The coupled microkinetic and transport models are then solved iteratively such that the flux of volatile species is consistent within the two models, given a fixed normalizing factor that is set through the roughness ρ parameter. This procedure corresponds in practice to optimizing the activity or concentration of near-surface species that enter the microkinetic or transport model, respectively. A more detailed description of the model is provided in the SI, Sec. S1.

Code & data availability

The code for the kinetic model, including all input model parameters used in this work, as well as the digitized reference data from the experimental literature will be made available pending publication.

Acknowledgments

We acknowledge support from the Federal Ministry of Education and Research, Germany in the framework of the project CatLab (03EW0015B), as well as the German Research Foundation (DFG) for funding through DFG CoE e-conversion EXC 2089/1. H.S.P. gratefully acknowledges the Alexander von Humboldt Foundation.

References

(1) Seh, Z. W.; Kibsgaard, J.; Dickens, C. F.; Chorkendorff, I.; Nørskov, J. K.; Jaramillo, T. F. Combining theory and experiment in electrocatalysis: Insights into materials design. *Science* **2017**, *355*.

(2) Nørskov, J.; Rossmeisl, J.; Logadottir, A.; Lindqvist, L.; Kitchin, J.; Bligaard, T.; Jónsson, H. Origin of the Overpotential for Oxygen Reduction at a Fuel-Cell Cathode. *J. Phys. Chem. B* **2004**, *108*, 17886–17892.

(3) Greeley, J.; Stephens, I.; Bondarenko, A.; Johansson, T. P.; Hansen, H. A.; Jaramillo, T.; Rossmeisl, J.; Chorkendorff, I.; Nørskov, J. K. Alloys of platinum and early transition metals as oxygen reduction electrocatalysts. *Nat. Chem.* **2009**, *1*, 552–556.

(4) Kulkarni, A.; Siahrostami, S.; Patel, A.; Nørskov, J. K. Understanding Catalytic Activity Trends in the Oxygen Reduction Reaction. *Chem. Rev.* **2018**, *118*, 2302–2312.

(5) Bagger, A.; Ju, W.; Varela, A. S.; Strasser, P.; Rossmeisl, J. Electrochemical CO_2 reduction: a classification problem. *ChemPhysChem* **2017**, *18*, 3266–3273.

(6) Tran, K.; Ulissi, Z. W. Active learning across intermetallics to guide discovery of electrocatalysts for CO_2 reduction and H_2 evolution. *Nat. Catal.* **2018**, *1*, 696–703.

(7) Zhong, M. et al. Accelerated discovery of CO_2 electrocatalysts using active machine learning. *Nat.* **2020**, *581*, 178–183.

(8) Kas, R.; Yang, K.; Bohra, D.; Kortlever, R.; Burdyny, T.; Smith, W. A. Electrochemical CO_2 reduction on nanostructured metal electrodes: fact or defect? *Chem. Sci.* **2020**, *11*, 1738–1749.

(9) Govindarajan, N.; Kastlunger, G.; Heenen, H. H.; Chan, K. Improving the intrinsic

activity of electrocatalysts for sustainable energy conversion: where are we and where can we go? *Chem. Sci.* **2022**, *13*, 14–26.

(10) Modestino, M. A.; Hashemi, S. M. H.; Haussener, S. Mass transport aspects of electrochemical solar-hydrogen generation. *Energy Environ. Sci.* **2016**, *9*, 1533–1551.

(11) Burdyny, T.; Smith, W. A. CO_2 reduction on gas-diffusion electrodes and why catalytic performance must be assessed at commercially-relevant conditions. *Energy Environ. Sci.* **2019**, *12*, 1442–1453.

(12) Suter, S.; Haussener, S. Optimizing mesostructured silver catalysts for selective carbon dioxide conversion into fuels. *Energy Environ. Sci.* **2019**, *12*, 1668–1678.

(13) Guo, J.; Brimley, P.; Liu, M. J.; Corson, E. R.; Muñoz, C.; Smith, W. A.; Tarpeh, W. A. Mass Transport Modifies the Interfacial Electrolyte to Influence Electrochemical Nitrate Reduction. *ACS Sustainable Chem. Eng.* **2023**,

(14) Ma, M.; Deng, W.; Xu, A.; Hochfilzer, D.; Qiao, Y.; Chan, K.; Chorkendorff, I.; Seger, B. Local reaction environment for selective electroreduction of carbon monoxide. *Energy Environ. Sci.* **2022**, *15*, 2470–2478.

(15) Jusys, Z.; Kaiser, J.; Behm, R. Methanol electrooxidation over Pt/C fuel cell catalysts: dependence of product yields on catalyst loading. *Langmuir* **2003**, *19*, 6759–6769.

(16) Wang, H.; Jusys, Z.; Behm, R. Ethanol electrooxidation on a carbon-supported Pt catalyst: reaction kinetics and product yields. *J. Phys. Chem. B* **2004**, *108*, 19413–19424.

(17) Seidel, Y.; Schneider, A.; Jusys, Z.; Wickman, B.; Kasemo, B.; Behm, R. Mesoscopic mass transport effects in electrocatalytic processes. *Faraday Discuss.* **2009**, *140*, 167–184.

(18) Mistry, H.; Behafarid, F.; Reske, R.; Varela, A. S.; Strasser, P.; Roldan Cuenya, B. Tuning catalytic selectivity at the mesoscale via interparticle interactions. *ACS Catal.* **2016**, *6*, 1075–1080.

(19) Wang, X.; Varela, A. S.; Bergmann, A.; Kühl, S.; Strasser, P. Catalyst particle density controls hydrocarbon product selectivity in CO_2 electroreduction on CuO_x. *ChemSusChem* **2017**, *10*, 4642–4649.

(20) Grosse, P.; Yoon, A.; Rettenmaier, C.; Herzog, A.; Chee, S. W.; Roldan Cuenya, B. Dynamic transformation of cubic copper catalysts during CO_2 electroreduction and its impact on catalytic selectivity. *Nat. Commun.* **2021**, *12*, 6736.

(21) Lim, C.; Harrington, D.; Marshall, A. Effects of mass transfer on the electrocatalytic CO_2 reduction on Cu. *Electrochim. Acta* **2017**, *238*, 56–63.

(22) Jang, J.; Rüscher, M.; Winzely, M.; Morales-Guio, C. G. Gastight rotating cylinder electrode: Toward decoupling mass transport and intrinsic kinetics in electrocatalysis. *AIChE J.* **2022**, *68*, e17605.

(23) Watkins, N.; Schiffer, Z.; Lai, Y.; Musgrave III, C.; Atwater, H.; Goddard III, W.; Agapie, T.; Peters, J.; Gregoire, J. Hydrodynamics Change Tafel Slopes in Electrochemical CO_2 Reduction on Copper. *ACS Energy Lett.* **2023**, *8*, 2185–2192.

(24) Cussler, E. L. *Diffusion: mass transfer in fluid systems*; Cambridge university press, 2009.

(25) Heenen, H. H.; Kastlunger, G.; Shin, H.; Overa, S.; Gauthier, J. A.; Jiao, F.; Chan, K. The mechanism for acetate formation in electrochemical $CO_{(2)}$ reduction on Cu: selectivity with potential, pH, and nanostructuring. *Energy Environ. Sci.* **2022**, *15*, 3978–3990.

(26) Kuhl, K. P.; Cave, E. R.; Abram, D. N.; Jaramillo, T. F. New insights into the electrochemical reduction of carbon dioxide on metallic copper surfaces. *Energy Environ. Sci.* **2012**, *5*, 7050–7059.

(27) Hori, Y. *Modern aspects of electrochemistry*; Springer, 2008; pp 89–189.

(28) Bertheussen, E.; Verdaguer-Casadevall, A.; Ravasio, D.; Montoya, J. H.; Trimarco, D. B.; Roy, C.; Meier, S.; Wendland, J.; Nørskov, J. K.; Stephens, I. E.; Chorkendorff, I. Acetaldehyde as an intermediate in the electroreduction of carbon monoxide to ethanol on oxide-derived copper. *Angew. Chem. Int. Ed.* **2016**, *128*, 1472–1476.

(29) Liu, X.; Schlexer, P.; Xiao, J.; Ji, Y.; Wang, L.; Sandberg, R. B.; Tang, M.; Brown, K. S.; Peng, H.; Ringe, S.; Hahn, C.; Jaramillo, T. F.; Nørskov, J. K.; Chan, K. pH effects on the electrochemical reduction of $CO_{(2)}$ towards C_2 products on stepped copper. *Nat. Commun.* **2019**, *10*.

(30) Kastlunger, G.; Wang, L.; Govindarajan, N.; Heenen, H. H.; Ringe, S.; Jaramillo, T.; Hahn, C.; Chan, K. Using pH dependence to understand mechanisms in electrochemical CO reduction. *ACS Catal.* **2022**, *12*, 4344–4357.

(31) Kastlunger, G.; Heenen, H. H.; Govindarajan, N. Combining First-Principles Kinetics and Experimental Data to Establish Guidelines for Product Selectivity in Electrochemical CO_2 Reduction. *ACS Catal.* **2023**, *13*, 5062–5072.

(32) Huang, Y.; Handoko, A. D.; Hirunsit, P.; Yeo, B. S. Electrochemical reduction of CO_2 using copper single-crystal surfaces: effects of CO* coverage on the selective formation of ethylene. *ACS Catal.* **2017**, *7*, 1749–1756.

(33) Li, C. W.; Kanan, M. W. CO_2 reduction at low overpotential on Cu electrodes resulting from the reduction of thick Cu_2O films. *J. Am. Chem. Soc.* **2012**, *134*, 7231–7234.

(34) Bertheussen, E.; Hogg, T. V.; Abghoui, Y.; Engstfeld, A. K.; Chorkendorff, I.; Stephens, I. E. Electroreduction of CO on polycrystalline copper at low overpotentials. *ACS Energy Lett.* **2018**, *3*, 634–640.

(35) Wang, L.; Nitopi, S.; Wong, A. B.; Snider, J. L.; Nielander, A. C.; Morales-Guio, C. G.; Orazov, M.; Higgins, D. C.; Hahn, C.; Jaramillo, T. F. Electrochemically converting carbon monoxide to liquid fuels by directing selectivity with electrode surface area. *Nat. Catal.* **2019**, *2*, 702–708.

(36) Jiang, K.; Huang, Y.; Zeng, G.; Toma, F. M.; Goddard III, W. A.; Bell, A. T. Effects of surface roughness on the electrochemical reduction of CO_2 over Cu. *ACS Energy Lett.* **2020**, *5*, 1206–1214.

(37) De Gregorio, G. L.; Burdyny, T.; Loiudice, A.; Iyengar, P.; Smith, W. A.; Buonsanti, R. Facet-dependent selectivity of Cu catalysts in electrochemical CO_2 reduction at commercially viable current densities. *ACS Catal.* **2020**, *10*, 4854–4862.

(38) Rossi, K.; Buonsanti, R. Shaping Copper Nanocatalysts to Steer Selectivity in the Electrochemical CO_2 Reduction Reaction. *Acc. Chem. Res.* **2022**, *55*, 629–637.

(39) Gauthier, J. A.; Stenlid, J. H.; Abild-Pedersen, F.; Head-Gordon, M.; Bell, A. T. The role of roughening to enhance selectivity to C_{2+} products during CO_2 electroreduction on copper. *ACS Energy Lett.* **2021**, *6*, 3252–3260.

(40) Ji, Y.; Chen, Z.; Wei, R.; Yang, C.; Wang, Y.; Xu, J.; Zhang, H.; Guan, A.; Chen, J.; Sham, T.-K.; Luo, J.; Yang, Y.; Xu, X.; Zheng, G. Selective CO-to-acetate electroreduction via intermediate adsorption tuning on ordered Cu–Pd sites. *Nat. Catal.* **2022**, *5*, 251–258.

(41) Dorakhan, R. et al. A silver–copper oxide catalyst for acetate electrosynthesis from carbon monoxide. *Nat. Synth.* **2023**, *2*, 448—457.

(42) Jouny, M.; Luc, W.; Jiao, F. High-rate electroreduction of carbon monoxide to multi-carbon products. *Nat. Catal.* **2018**, *1*, 748–755.

(43) Luc, W.; Fu, X.; Shi, J.; Lv, J.-J.; Jouny, M.; Ko, B. H.; Xu, Y.; Tu, Q.; Hu, X.; Wu, J.; Yue, Q.; Jiao, F.; Kang, Y. Two-dimensional copper nanosheets for electrochemical reduction of carbon monoxide to acetate. *Nat. Catal.* **2019**, *2*, 423–430.

(44) Zhu, P.; Xia, C.; Liu, C.-Y.; Jiang, K.; Gao, G.; Zhang, X.; Xia, Y.; Lei, Y.; Alshareef, H. N.; Senftle, T. P.; Wang, H. Direct and continuous generation of pure acetic acid solutions via electrocatalytic carbon monoxide reduction. *Proc. Natl. Acad. Sci. U.S.A.* **2020**, *118*.

(45) da Silva, A. H. M.; Raaijman, S. J.; Santana, C. S.; Assaf, J. M.; Gomes, J. F.; Koper, M. T. M. Electrocatalytic CO_2 reduction to C_{2+} products on Cu and Cu_xZn_y electrodes: Effects of chemical composition and surface morphology. *J. Electroanal. Chem.* **2021**, *880*, 114750.

(46) Mittermeier, T.; Weiß, A.; Gasteiger, H. A.; Hasché, F. Monometallic palladium for oxygen reduction in PEM fuel cells: particle-size effect, reaction mechanism, and voltage cycling stability. *J. Electrochem. Soc.* **2017**, *164*, F1081.

(47) Karuppannan, M.; Kim, Y.; Gok, S.; Lee, E.; Hwang, J. Y.; Jang, J.-H.; Cho, Y.-H.; Lim, T.; Sung, Y.-E.; Kwon, O. J. A highly durable carbon-nanofiber-supported Pt–C core–shell cathode catalyst for ultra-low Pt loading proton exchange membrane fuel cells: facile carbon encapsulation. *Energy Environ. Sci.* **2019**, *12*, 2820–2829.

(48) Göhl, D.; Garg, A.; Paciok, P.; Mayrhofer, K. J.; Heggen, M.; Shao-Horn, Y.; Dunin-Borkowski, R. E.; Román-Leshkov, Y.; Ledendecker, M. Engineering stable electrocatalysts by synergistic stabilization between carbide cores and Pt shells. *Nat. Mater.* **2020**, *19*, 287–291.

(49) Kolle-Görgen, E.; Fortunato, G.; Ledendecker, M. Catalyst Stability in Aqueous Electrochemistry. *Chem. Mater.* **2022**, *34*, 10223–10236.

(50) Huang, J.; Hörmann, N.; Oveisi, E.; Loiudice, A.; De Gregorio, G. L.; Andreussi, O.; Marzari, N.; Buonsanti, R. Potential-induced nanoclustering of metallic catalysts during electrochemical CO_2 reduction. *Nat. Commun.* **2018**, *9*, 3117.

(51) Virtanen, P. et al. SciPy 1.0: fundamental algorithms for scientific computing in Python. *Nat. Methods* **2020**, *17*, 261–272.